Electron scattering by atomic chains: Multiple-scattering effects

M.-L. Xu, J. J. Barton,* and M. A. Van Hove
Center for Advanced Materials, Materials and Chemical Sciences Division, Lawrence Berkeley Laboratory, Berkeley, California 94720
(Received 6 July 1988; revised manuscript received 17 November 1988)

Multiple-scattering effects of electrons traveling along atomic chains are shown to be important and useful for surface structure determination, especially in the medium-energy range (200–1000 eV). This applies to techniques based on diffraction of elastic electrons, such as medium-energy electron diffraction, as well as to techniques based on the angle-resolved detection of "secondary" electrons such as photoelectrons, Auger electrons, and other electrons. Two new methods for computing multiple-scattering amplitudes for chains are derived and used to show how multiple scattering along chains of atoms produces focusing, defocusing, amplification, and layer-dependent enhancements that can be put to effective use in structure determination. Strong forward-focusing peaks along internuclear axes are dominant under many conditions: this is a single-scattering effect. However, multiple scattering can totally defocus such forward-focused peaks, while other interference effects produce additional scattering peaks that do not have the direction of an internuclear axis. In addition, it follows that surface composition analysis by conventional Auger-electron spectroscopy can be quite sensitive to the incident direction of the electron beam used to produce Auger emission.

I. INTRODUCTION

Chains of aligned atoms occur in many situations: obvious examples are provided by crystals and long or short straight molecules. Electron scattering by such structures is an important aspect of surface-science studies with a variety of electron-based techniques. The scattering of electrons by chains of atoms is especially important in techniques that provide surface structural information, including the diffraction methods and the fine-structure methods: low-energy electron diffraction[1–3] (LEED) and its higher-energy counterparts—medium-energy and reflection high-energy electron diffraction (MEED and RHEED);[4–6] angle-resolved photoemission extended fine structure (ARPEFS),[7–10] surface-extended x-ray-absorption fine structure (SEXAFS),[11,12] extended appearance-potential fine structure (EAPES),[13] and surface-extended energy-loss fine structure (SEELFS),[14] to name some of the major ones. Recently, forward focusing of electrons by surface atoms has also emerged as a very useful tool for structural determination and clearly involves the scattering along chains of atoms.[15–24]

Also of interest is the possibility of focusing effects in standard Auger electron spectroscopy induced by electrons: the incident electrons may be focused preferentially onto certain atomic layers of the surface, giving rise to a layer-dependent Auger-electron yield, over and above the conventional mean-free-path effect.

Previous theoretical work with photoemission scattering[9] and medium-energy electron diffraction[25,26] has shown the key role of chains of atoms in the understanding of electron multiple scattering in the intermediate-energy range. At all energies, electron multiple scattering is likely to occur. At low electron kinetic energies, say below 100 eV, the scattering by a single atom is unfocused, i.e., the electron emerges without a strong preference for a particular direction. But, as the energy is raised above 100 eV, the scattering becomes increasingly focused in the forward direction. For instance, at an energy of about 1000 eV a metal atom focuses an electronic plane wave into a cone that has a half-width of approximately 10°. Thus, multiple scattering at medium energies is most prevalent when multiple forward scattering is possible, as in the linear chains we will study here.

In this paper our aim is to explore the nature of multiple scattering of electrons along atomic chains in the energy range 200–1000 eV. We shall set up an efficient calculational scheme and apply it to simple but realistic situations that impact on surface-structure determination. Elsewhere,[23,24] we shall exploit our findings to develop further the understanding and use of forward focusing for actual surface crystallography.

Two principal situations must be considered: the scattering electrons originate from far away, as in electron diffraction, or they originate in the chain itself, as in the emission of secondary electrons, such as photoelectrons or Auger electrons, or in the inelastic scattering of electrons. In the first case we shall assume an incident plane wave hitting all atoms of the chain. In the second case we shall assume a spherical wave emitted from an atom at one end of the chain.

In Secs. II–IV we shall develop the necessary theoretical formalism. We start with single scattering in Sec. II, then include multiple scattering self-consistently in Sec. III. A more efficient calculational scheme will be presented in Sec. IV.

In Sec. V we summarize the important aspects of electron scattering by single isolated atoms. In Sec. VI the theory will be applied to chains of atoms, first from a

point source of electrons, and then from a distant source of electrons. In Sec. VII we shall discuss the significance and potential uses of the scattering properties of electrons along chains.

II. CHAIN GEOMETRY AND FIRST-ORDER WAVES

Our scattering system consists of a linear chain of N muffin-tin potentials, labeled 0 to $N-1$ and spaced by a constant vector $\mathbf{a}$. For our methods it is essential to select the $\hat{\mathbf{z}}$ axis of the coordinate system for the scattering calculation parallel to the chain axis; $+\hat{\mathbf{z}}$ will point into the chain.

We define two arrays with index l,

$$[\mathbf{w}_m(k\mathbf{r}_n)]_l=\frac{1}{ik}d_l(kr_n)Y_{lm}(\hat{\mathbf{r}}_n),\quad l=|m|,\ldots,l_{\max}$$
$$[\mathbf{v}_m(\mathbf{k}_{\rm in})]_l=4\pi T_l(k)Y^*_{lm}(\hat{\mathbf{k}}_{\rm in}),\quad l=|m|,\ldots,l_{\max}\quad(1)$$

so that an incoming plane wave with wave vector $\mathbf{k}_{\rm in}$ scattering upon the nth atom of the chain may be written as

$$\psi_1^{(n)}(\mathbf{r})=e^{i\mathbf{k}_{\rm in}\cdot n\mathbf{a}}\frac{e^{ikr_n}}{r_n}\sum_{m=-l_{\max}}^{l_{\max}}\mathbf{w}_m^T(k\mathbf{r}_n)\mathbf{v}_m\ .$$

The function d_l is a polynomial in $(1/2ikr)$ discussed in Ref. 8 and it asymptotically approaches 1 for $kr\gg l(l+1)/2$. This polynomial is important for quantitative near-field curved-waved calculations, but the basic spherical-wave nature of the spherical Bessel functions h_l is carried in the asymptotic part. The other functions including the convention chosen for the spherical harmonics is detailed in Ref. 7.

The complete single-scattered wave function for a detector at $\mathbf{R}$ where $|\mathbf{R}|\gg|\mathbf{a}|$ may be derived by summing waves from all N atoms using $|\mathbf{R}_n|=|\mathbf{R}_n-n\mathbf{a}|\approx|\mathbf{R}|-n\mathbf{a}\cdot\hat{\mathbf{R}}$:

$$\Psi_1^{(N)}(\mathbf{R})=\frac{e^{ikR}}{R}\sum_{n=0}^{N-1}(e^{i\mathbf{k}_{\rm in}\cdot n\mathbf{a}}e^{-ik\hat{\mathbf{R}}\cdot n\mathbf{a}})\times\sum_{m=-l_{\max}}^{l_{\max}}\mathbf{w}_m^T(k\mathbf{R})\mathbf{v}_m\ .$$

The vector $\mathbf{w}_m$ is now independent of n and we may recognize the atomic scattering factor

$$\sum_{m=-l_{\max}}^{l_{\max}}\mathbf{w}_m^T\mathbf{v}_m=\frac{1}{ik}\sum_{l=0}^{l_{\max}}(2l+1)T_l(k)P_l(\cos\theta_{\mathbf{k}_{\rm in}\cdot\mathbf{R}})=f_{\mathbf{k}_{\rm in}\cdot\mathbf{R}}\ .$$

The measured intensity will be

$$\Psi_1^*\Psi_1=\frac{|f_{\mathbf{k}_{\rm in}\cdot\mathbf{R}}|^2}{R^2}\left[\left[\frac{1-e^{-i\Delta\mathbf{K}\cdot N\mathbf{a}}}{1-e^{-i\Delta\mathbf{K}\cdot\mathbf{a}}}\right]\left[\frac{1-e^{i\Delta\mathbf{K}\cdot N\mathbf{a}}}{1-e^{i\Delta\mathbf{K}\cdot\mathbf{a}}}\right]\right].$$

where $\Delta\mathbf{K}=\mathbf{k}_{\rm in}-k\hat{\mathbf{R}}$. The structure factor in large square brackets will be equal to N^2 for $\Delta\mathbf{K}\cdot\mathbf{a}=2\pi j$, $j=0,\pm1,\pm2,\pm3,\ldots$, but of order 1 for other values of $\Delta\mathbf{K}$. This is the Bragg-like condition for chains and it leads to cones of emission maxima about the chain axis. Superimposed on these cones of intensity will be the atomic-scattering factor $|f(\theta)|$ which will favor forward (along $\mathbf{k}_{\rm in}$) scattering for all but the lowest electron energies.

For spherical-wave emission with components A_{lm}, we define

$$[\mathbf{p}_m]_l=A_{lm},\quad l=|m|,\ldots,l_{\max}\ .$$

Then the first-order wave function scattered from atom n at the detector can be expressed as

$$\phi_1^{(n)}(\mathbf{R})=\frac{e^{ikR}}{R}e^{-ikn\mathbf{a}\cdot\hat{\mathbf{R}}}\sum_{m=-l_{\max}}^{l_{\max}}\mathbf{w}_m^T(k\mathbf{R})\mathbf{p}_m\ .$$

III. MULTIPLE SCATTERING WITH NOZAWA'S ORIGIN-SHIFT THEOREM

Our next task is to include multiple-scattering terms in the chain scattering. All such terms will involve the propagation of expanding spherical waves from one atom to another. Therefore, the wave field must be expressed in terms of incoming spherical waves. The Nozawa origin-shift theorem[27] describes an outgoing wave centered at the point $n\mathbf{a}$ in terms of waves about $n'\mathbf{a}$, where $\mathbf{a}\|\hat{\mathbf{z}}$ by

$$i^l h_l(kr_n)Y_{lm}(\hat{\mathbf{r}}_n)=\frac{e^{ik|n-n'|a}}{ik|n-n'|a}\sum_{l'=m}^{\infty}D_{ll'}^m[k(n'-n)\mathbf{a}]\times i^{l'}j_{l'}(kr_{n'})Y_{l'm}(\hat{\mathbf{r}}_{n'})\ ,$$

where we have factored out the asymptotic limit from Nozawa's $H_{ll'}^m$:

$$4\pi N_{lm}N_{l'm}H_{ll'}^m(ka)=\frac{e^{ika}}{ika}D_{ll'}^m(ka)\ .$$

The quantities $D_{ll'}^m$ are related to the usual Gaunt-integral coefficients as our d_l is related to the spherical Hankel functions; simple recursion relations for the $D_{ll'}^m$ can be derived[28] from the formulas given by Nozawa.

To simplify our notation, we define a propagating matrix whose l,l' element is

$$[\mathbf{H}_m(n'-n)]_{ll'}=\frac{e^{ik|n'-n|a}}{ik|n'-n|a}T_l(k)D_{ll'}^m(k(n'-n)a)\ .$$

This matrix takes (l,m) outgoing waves on center n, scatters them from center n', and gives the amplitude of outgoing waves on center n' of type (l',m); it is defined for $m\le l,l'\le l_{\max}$. Then we assemble the propagating matrices into a scattering supermatrix $\mathbf{X}_m$ with matrix entries

$$[\mathbf{X}_m]_{n'n}=\begin{cases}\mathbf{H}_m(n'-n) & \text{if } n'\neq n\ ,\\ 0 & \text{if } n'=n\ .\end{cases}$$

Next, we define the nth component of the composite vector $\mathbf{y}_{m_j}$ to be the vector of partial-wave amplitudes existing from atom n after j scattering events. We have

$$[\mathbf{y}_{m_1}]_n = e^{i\mathbf{k}_{\rm in}\cdot n\mathbf{a}}\mathbf{v}_m \ .$$

Similarly, for emission from a point source we use

$$[\hat{\mathbf{z}}_{m_1}]_n = \begin{cases} \mathbf{p}_m & \text{if the } n\text{th atom is excited ,} \\ 0 & \text{otherwise .} \end{cases}$$

Finally, the composite vector $\mathbf{d}_m(\mathbf{r})$ contains outgoing partial wavelets:

$$[\mathbf{d}_m(\mathbf{r})]_n^T = \frac{e^{ikr_n}}{r_n}\mathbf{w}_m^T(kr_n) \ , \tag{2}$$

which can be weighted by the partial-wave amplitude in $\mathbf{y}_m$ and summed to give the complete wave function:

$$\Psi_1^{(N)}(\mathbf{r}) = \sum_{m=-l_{\rm max}}^{l_{\rm max}} d_m^T(\mathbf{r})\mathbf{y}_{m_1}(\mathbf{k}_{\rm in}) \ .$$

With these definitions, the second-order wave is

$$\Psi_2^{(N)}(\mathbf{r}) = \sum_{m=-l_{\rm max}}^{l_{\rm max}} d_m^T(\mathbf{r})\mathbf{X}_m\mathbf{y}_{m_1} \tag{3}$$

for incident plane waves (i.e., double scattering) and

$$\Psi_2^{(n)}(\mathbf{r}) = \sum_{m=-l_{\rm max}}^{l_{\rm max}} d_m^T(\mathbf{r})\mathbf{X}_m\mathbf{z}_{m_1}$$

for a point source (i.e., single scattering). We exclude the zero-distance scattering case ($n'=n$) by defining $\mathbf{H}_m(0)=\mathbf{0}$.

The parallel form of these equations is already evident; we may extend them to higher-order scattering by inspection. The iterative form of these equations may be exploited to give an "exact" full order wave function:

$$\Psi_\infty^{(N)}(\mathbf{r}) = \sum_{m=-l_{\rm max}}^{l_{\rm max}} \mathbf{d}_m^T(\mathbf{r})(\mathbf{I}-\mathbf{X}_m)^{-1}\mathbf{y}_{m_1} \ ,$$

and similarly for Φ_∞ with $\mathbf{z}_{m_1}$ in place of $\mathbf{y}_{m_1}$.

The equations above are valid anywhere outside of the muffin-tin potentials. When we evaluate the wave amplitude at our distant detector position $\mathbf{R}$, we approximate

$$\frac{e^{ikr_n}}{r_n} \to \frac{e^{ikR}}{R}e^{-ik\hat{\mathbf{R}}\cdot n\mathbf{a}} \quad \text{and} \quad \mathbf{w}_m(k\mathbf{r}_n)\to\mathbf{w}_m(k\mathbf{R}) \ .$$

We can then multiply and divide by powers of $e^{i\mathbf{k}_{\rm in}\cdot\mathbf{a}}$. This gives us a new propagation matrix,

$$\tilde{\mathbf{H}}_m(\Delta n) = e^{i\mathbf{k}_{\rm in}\cdot\Delta n\,\hat{\mathbf{a}}}\mathbf{H}_m(\Delta n) \ ,$$

which is directly analogous to the usual definition chosen[1] for two-dimensional LEED scattering problems. This is advantageous for plane-wave scattering from an infinite chain since the sums over scattered waves from other atoms are expressed solely in terms of differences in position: we may use translational invariance to simplify the solution. For example, the third-order wave scattering from an infinite chain is

$$\Psi_3^\infty(\mathbf{R}) = \frac{e^{ikR}}{R}\left[\frac{1}{1-e^{i\mathbf{k}_{\rm in}\cdot\mathbf{a}-ik\hat{\mathbf{R}}\cdot\mathbf{a}}}\right] \times \sum_{m=-l_{\rm max}}^{l_{\rm max}} \mathbf{w}_m^T(k\mathbf{R})\mathbf{X}_m^\infty\mathbf{X}_m^\infty\mathbf{v}_m \ , \tag{4}$$

where $\mathbf{X}_m^\infty$ is given by

$$\mathbf{X}_m^\infty = \sum_{\Delta n=-\infty}^{+\infty} \tilde{\mathbf{H}}_m(\Delta n) \ . \tag{5}$$

The full-order solution is

$$\Psi_\infty^{(\infty)}(\mathbf{R}) = \frac{e^{ikR}}{R}\left[\frac{1}{1-e^{i\mathbf{a}\cdot(\mathbf{k}_{\rm in}-k\hat{\mathbf{R}})}}\right] \times \sum_{m=-l_{\rm max}}^{l_{\rm max}} \mathbf{w}_m^T(\mathbf{I}-\mathbf{X}_m^\infty)^{-1}\mathbf{v}_m \ .$$

We note that for every formula in this section we can avoid half of the numerical work by combining negative and positive values of m.

The formulas in this section are no more than the well-known LEED formulas adopted to the chain geometry. They are, however, much more efficient for numerical calculation. The chain version requires $m_{\rm max}$ matrix inversions ($\mathbf{X}_m$ does not depend on the sign of m), each of which requires of order $(l_{\rm max}+1)^3$ operations. Solution by the more general method would require only one inversion, but the matrix would have dimension $(l_{\rm max}+1)^2$ by $(l_{\rm max}+1)^2$: the inverse requires of order $(l_{\rm max}+1)^6$ computations. Hence the special-case formulas are $(l_{\rm max}+1)^2$ times less expensive when $m_{\rm max}=l_{\rm max}$, a consideration of great importance when $l_{\rm max}$ reaches 10 or more. Furthermore, $m_{\rm max}$ can, in fact, be much less than $l_{\rm max}$, so that the advantage of the chain formulas increase with energy.

IV. CHAIN SCATTERING WITH THE TAYLOR-SERIES MAGNETIC-QUANTUM-NUMBER EXPANSION

The formulation in the preceding section relies upon specialization of an exact origin-shift addition theorem. Recently, a new addition theorem for spherical waves—called the Taylor-series magnetic-quantum-number expansion (TS-MQNE)—has been derived,[29] which corresponds to a finite series summing to an exact result.

We start with scattering matrices for incoming partial waves,

$$[\mathbf{C}_m]_{pl''}(\sigma_{nn'}) = N_{l''m}\sigma_{nn'}^{l''+m}c_{pm}^{l''} \ ,$$

and outgoing partial waves,

$$[\mathbf{G}_m(n-n')]_{pl} = 4\pi\frac{T_l}{ik}H_l^{p|m|}(k|n-n'|a)N_{lm}(\sigma_{nn'})^{l+m} \ ,$$

where

$$\sigma_{nn'}^{l+l'} = \begin{cases} (-1)^{l+l'} & \text{if } n<n' \ , \\ (1) & \text{otherwise ,} \end{cases}$$

so that

$$\mathbf{H}_m(k(n-n')a)=\frac{e^{ik|n-n'|a}}{|n-n'|a}\mathbf{G}_m^T(n-n')\mathbf{C}_m(\sigma_{nn'}) . \quad (6)$$

The remaining quantities are defined in Ref. 7, where simple recursion relations are given for the integrals $H_{ll'}^{p|m|}(k|n-n'|a)$.

The product of $\mathbf{C}_m$ and $\mathbf{G}_m$ contains sums on the Taylor-series parameter p. We have decomposed the $l\times l''$ propagation matrix $\mathbf{H}_m$ into an $l\times p$ part and a $p\times l''$ part. By inserting this expression wherever $\mathbf{H}_m$ appears in the preceding section and summing over partial waves (l and l''), we may convert the chain formulas based on Nozawa's method into scattering-factor formulas. This conversion transforms each part of the chain-scattering formulas from an orbital-angular-momentum basis to a Taylor-series basis.

We begin by defining the transformed parts. The incoming partial-wave amplitudes in $\mathbf{y}_{m_j}$ become incoming-wave scattering factors:

$$[\mathbf{n}_{m_j}]_{\pm n}=\mathbf{C}_m(\pm)[\mathbf{y}_{m_j}]_n ,$$

and the outgoing-wavelet amplitudes become outgoing-wave scattering factors:

$$[\mathbf{o}_{m_j}]_{+n}=\sum_{n'=n+1}^{N}\frac{e^{ik|n-n'|a}}{|n-n'|a}\mathbf{G}_m(n-n')[\mathbf{d}_m]_{n'} ,$$

$$[\mathbf{o}_{m_j}]_{-n}=\sum_{n'=0}^{n-1}\frac{e^{ik|n-n'|a}}{|n-n'|a}\mathbf{G}_m(n-n')[\mathbf{d}_m]_{n'} .$$

The plus and minus signs refer to wave components traveling up and down the chain, respectively. We use these definitions when we insert our decomposed $\mathbf{H}_m$ into the double-scattered wave function, Eq. (3), giving

$$\Psi_2^{(N)}=\sum_{m=-l}^{l}\mathbf{o}_m^T\mathbf{n}_{mj} .$$

Third- and higher-order waves require a scattering-factor matrix,

$$\mathbf{F}_m(n'-n,\pm n')=\mathbf{C}_m(\pm n')\mathbf{G}_m^T(n'-n)\frac{e^{ik|n-n'|a}}{|n-n'|a} ,$$

which we assemble into a supermatrix $\mathbf{Z}_m$ to parallel $\mathbf{X}_m$ from the preceding section:

$$[\mathbf{Z}_m]_{\pm n,\pm n'}=\begin{cases}\mathbf{F}_m(n'-n,\pm n') & \text{if } 0<|n-n'|<N ,\\ 0 & \text{otherwise} ,\end{cases}$$

giving, for example, the third-order wave function as

$$\Psi_3^{(N)}=\sum_{m=-l}^{l}\mathbf{o}_m^T\mathbf{Z}_m\mathbf{n}_m . \quad (7)$$

Each entry in the matrix $\mathbf{F}_m$ and in the vectors $\mathbf{o}_m$ and $\mathbf{n}_m$ are generalized scattering factors described in Ref. 9. Specifically,

$$[\mathbf{F}_m(n'-n,\pm n')]_{pp'}=\frac{e^{ik|n-n'|a}}{|n-n'|a}F_{pm}^{p'm}(k,(n'-n)\mathbf{a},\pm\hat{\mathbf{a}}) ,$$

$$[\mathbf{o}_m(-n)]_p=\sum_{n'=0}^{n'-1}\frac{e^{ik|n-n'|a}}{|n-n'|a}F_{pm}^{00}(k,(n'-n)\mathbf{a},\hat{\mathbf{R}}) ,$$

$$[\mathbf{o}_m(+n)]_p=\sum_{n'=n+1}^{N}\frac{e^{ik|n-n'|a}}{|n-n'|a}F_{pm}^{00}(k,(n'-n)\mathbf{a},\hat{\mathbf{R}}) ,$$

and

$$[\mathbf{n}_m(\pm n)]_{p'}=F_{00}^{p'm}(k,\hat{\mathbf{k}}_{\text{in}},(\pm n)\hat{\mathbf{a}}) .$$

These scattering factors give the amplitude for spherical-wave components (p,m) on one atom to propagate along $\mathbf{a}$ and scatter from a second atom into the direction $\pm\hat{\mathbf{a}}$:

$$F_{pq}^{p'q'}(k,(n-n')\mathbf{a},(n'-n'')\hat{\mathbf{a}})=\delta_{qq'}(-1)^q\frac{1}{ik}\sum_{l=|q|}^{l_{\max}}\left[(2l+1)T_l(k)\sigma_{n-n',n'-n''}^{l}H_l^{pq}(k|n-n'|a)\frac{(l-|q|)!}{(l+|q|)!}c_{p'q}^{l}\right] .$$

When we compare our new result for the triple-scattered wave from a chain to the method of the preceding section, we can understand the differences introduced by the scattering-factor method. The basis for the Nozawa formulation of the preceding section consists of partial waves: the elements of the vectors $\mathbf{y}_m$ and $\mathbf{d}_m$ are orbital-angular-momentum components of wave amplitude on each atom. Hence the length of these vectors is equal to $l_{\max}+1$ times the number of atoms. For the TS-MQNE method, the elements of the $\mathbf{o}_m$ and $\mathbf{n}_m$ vectors are spherical-wave components of scattering amplitude. These elements are associated with particular directions, either up or down the chain. Each atom in the chain can scatter either into $+\hat{\mathbf{z}}$ or $-\hat{\mathbf{z}}$ directions, except for the end atoms, which are restricted to only one direction. Thus, $2n-2$ scattering directions are required. If we call $\tau+1$ the maximum number of components with index p that are required to accurately represent the scattering, then we will need $(\tau+1)(2N-2)$ elements in $\mathbf{o}_m$ and $\mathbf{n}_m$. Previous experience[9] shows that $\tau\leq 2$ is quite accurate for medium-energy electron scattering and that the required value of τ falls quickly to zero for long scattering distances and large scattering angles. Hence the length of the vectors in the TS-MQNE formulation is equal to a small number times the number of atoms in the chain. From this analysis we can conclude that the TS-MQNE method will be advantageous for medium and high energy $[l_{\max}>2(\tau+1)]$.

In addition to using the TS-MQNE in the scattered-wave formulas, we can also seek a full-order wave function. Successive incoming-wave scattering factors are related by the iterative formula

$$\mathbf{n}_{m_j+1}=\mathbf{Z}_m\mathbf{n}_{m_j} .$$

By summing this recursion, we find simultaneous equa-

tions for the full-order scattering vectors $\mathbf{n}_{m_\infty}$ which may be formally solved to give the full-order solution for a finite-length chain using the TS-MQNE as

$$\Psi_\infty^{(N)} = f(\theta_{\mathbf{k}_{\rm in}\cdot\hat{\mathbf{R}}}) \sum_{n=0}^{N-1} e^{i(\mathbf{k}_{\rm in}-k\hat{\mathbf{R}})\cdot n\mathbf{a}} + \sum_{m=-l}^{l} \mathbf{o}_m^T (\mathbf{I}-\mathbf{Z}_m)^{-1}\mathbf{n}_{m_1} .$$

The first term is the single-scattered wave, which requires no curved-wave correction.

Parallel with our development in Sec. III, we conclude with the infinite-chain case. Translational symmetry allows us to concentrate on a single atom with scattering components in the $+\hat{\mathbf{z}}$ and $-\hat{\mathbf{z}}$ directions. The matrix $\mathbf{Z}_m^\infty$ will have four submatrices,

$$[\mathbf{Z}_m^\infty]_{\pm,\pm} = \sum_{n=1}^{\infty} \frac{e^{ikna}}{na} \mathbf{F}_m(k, \pm\mathbf{a}, \pm\hat{\mathbf{a}}) ,$$

with the wave-function radial decay and inelastic scattering contributing to the convergence of the sum. This sum and Eq. (5) will require a similar number of terms, but each term in Eq. (5) is an $(l_{\max}+1)\times(l_{\max}+1)$ matrix. The terms here for $\mathbf{Z}_m$ are $(\tau+1)\times(\tau+1)$ matrices, and the size of the matrices falls rapidly as the sum progresses, leading to a single complex number. The solution is

$$\Psi_\infty^\infty = \left[\frac{1}{1-e^{i(\mathbf{k}_{\rm in}-k\hat{\mathbf{R}})\cdot\mathbf{a}}}\right] \times \left[f(\theta_{\mathbf{k}_{\rm in}\cdot\hat{\mathbf{R}}}) + \sum_{m=-l}^{l} \mathbf{o}_m^T (\mathbf{I}-\mathbf{Z}_m^\infty)^{-1}\mathbf{n}_{m_1}\right] .$$

Thus we have another solution to the chain multiple-scattering problem.

As was the case for the Nozawa method, the scattering matrix $\mathbf{Z}_m$ has a special structure which can be used to advantage for practical computations. For a chain with N atoms the matrix has $(2N-2)^2$ submatrices, of which half are zero and only $2N-1$ are unique. The matrix can be partitioned into four banded triangular matrices which can be identified as two identical forward-scattering matrices and two identical backscattering matrices. This structure should facilitate perturbation-scattering methods of solving the chain-scattering problem.

V. ELECTRON SCATTERING BY ONE ATOM

The properties of electron scattering by a single atom are fundamental to our discussion. The atom acts on the passing electron like a crude converging electrostatic lens, see Figs. 1(a) and 1(b). In Fig. 2 we illustrate the atomic-scattering amplitude $f(\theta)$ for nickel and oxygen atoms at a few energies of interest to us. The forward-scattering peak is seen to sharpen strongly toward higher energies, while scattering in other directions decreases appreciably.

We now explore how multiple scattering from atom to atom in a chain takes place and affects the resulting angular distribution of scattered electrons.

VI. ELECTRON SCATTERING ALONG ATOMIC CHAINS

The physical parameters used in our calculations are the same as for conventional LEED calculations, extended where appropriate to energies on the order of 1000 eV. We used up to 20 phase shifts, which are based on Moruzzi-Janak-Williams potentials[30] for nickel and copper, and on Tong-Puga surface potentials[31] from Herman-Skillman wave functions for carbon and oxygen in carbon monoxide. The electron mean free path was set to 24 Å. Isotropic, layer-independent thermal vibrations were included, corresponding to Debye temperatures of 335 K for nickel, 343 K for copper, 1405 K for carbon, and 1217 K for oxygen, with an actual temperature of 300 K.

A. Point source in chain

We first consider the case of a source atom located at the end of the chain. It emits an electron as an s wave, which will be scattered by the complete chain. We plot the angular distribution of the emitted and scattered wave amplitudes taken together. The length of the chain is varied from two atoms to many atoms. To simulate emission from a fcc (100) crystal surface, the chain is tilted by 45° with respect to the surface, and damping is included from the surface plane down into the otherwise atom-free bulk. Thus the angular distribution will not have exactly cylindrical symmetry about the chain axis.

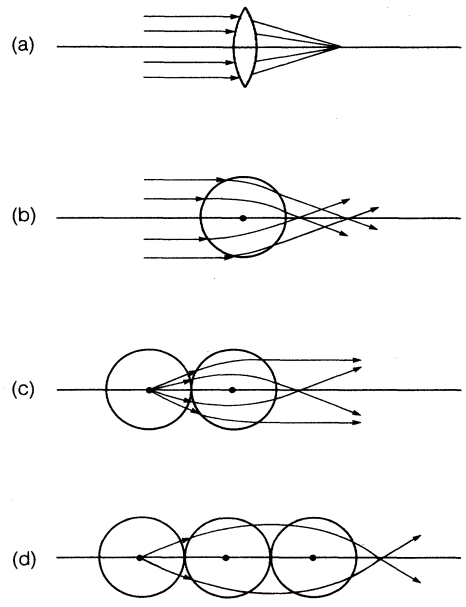

FIG. 1. (a) Optical paths for forward focusing of incident parallel light by a lens. (b) Classical trajectories for forward focusing of parallel beam of electrons by one atom. (c) Same as (b), but for electrons emitted from a point source. (d) Same as (c), but with forward focusing by two atoms.

The top of Fig. 3 shows the resulting angular distribution for a chain of two copper atoms at 917 eV. One recognizes the dominant effect of the atomic-scattering amplitude as a strong forward-scattering peak, cf. Fig. 2 (copper and nickel have almost identical atomic-scattering amplitudes). However, there are new secondary peaks to either side of the main forward peak. These are interference peaks between the unscattered emitted s wave and the scattered wave coming from the other atom, as discussed before.[32]

Figure 3 also shows the effect of removing multiple scattering between the two atoms, which in this geometry and at high energies consists of very weak back-and-forth scattering.

The case of three atoms in the chain is shown in the middle of Fig. 3. The central forward-scattering peak is slightly sharper, but markedly smaller. It loses intensity due to defocusing: electrons are focused by the second atom in the chain onto the third atom; the third atom, in turn, tries to converge the electron trajectories, but overdoes it, as schematically illustrated with trajectories in Figs. 1(c) and 1(d).

Defocusing is perhaps the most important effect of multiple scattering in atomic chains. Single-scattering theories predict large forward peaks which can be decreased drastically by defocusing, and even destroyed completely in longer chains, as we shall see presently. A multiple-scattering treatment is essential to properly model this effect.

As Fig. 3 shows, the three-atom chain also exhibits disturbances in the secondary nonforward peaks, compared to the two-atom chain. These are simply due to additional interfering trajectories. The five-atom chain gives the angular distribution shown at the bottom of Fig. 3. The forward peak has almost vanished due to repeated defocusing along the chain.

We next show that lighter atoms, such as those common in molecules, can produce similar focusing effects. Figure 4 exhibits the angular distribution of a single two-atom chain of carbon monoxide, where carbon acts as the s-wave emitter. Again, the atomic-scattering amplitude gives rise to a distinctive forward peak, while interference

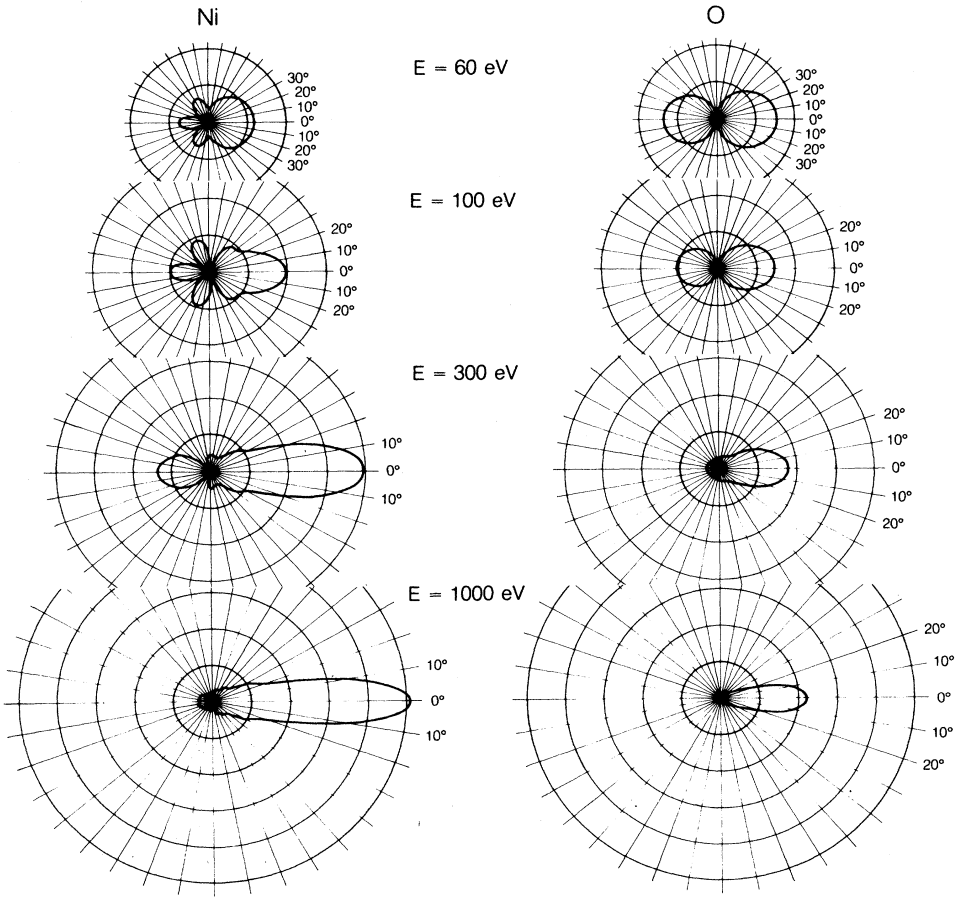

FIG. 2. Atomic-scattering amplitude $|f(\theta)|$ for nickel and oxygen atoms at a few energies. The forward direction is defined as $\theta=0°$.

effects create secondary peaks. The forward peak, however, has a larger half-width, in tune with the atomic-scattering amplitude, cf. Fig. 2.

B. Incident plane wave

With an incident plane wave we have a more complex problem. In addition to the multiple scattering of electrons out of the crystal, as we discussed for the point source in the preceding section, we have two further effects. First, all the atoms in the chain are excited coherently by the incident plane. This introduces additional interference structure (Bragg-like features) into the final result; the added structure is well understood even in the multiple-scattering case.[26] Second, the incident wave

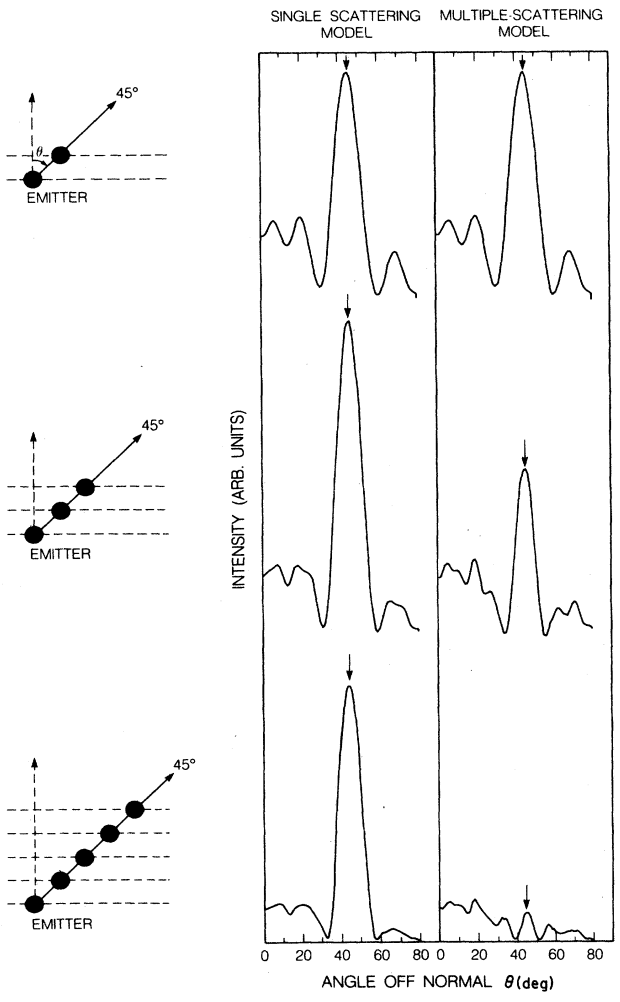

FIG. 3. Polar-angle intensity distribution for Cu Auger emission at $E = 917$ eV from a point source at the end of a Cu chain, calculated with single scattering and with multiple scattering. The left-hand diagrams illustrate the chain geometry used for each calculation. Vertical arrows in two right-hand panels indicate the forward-focusing peaks.

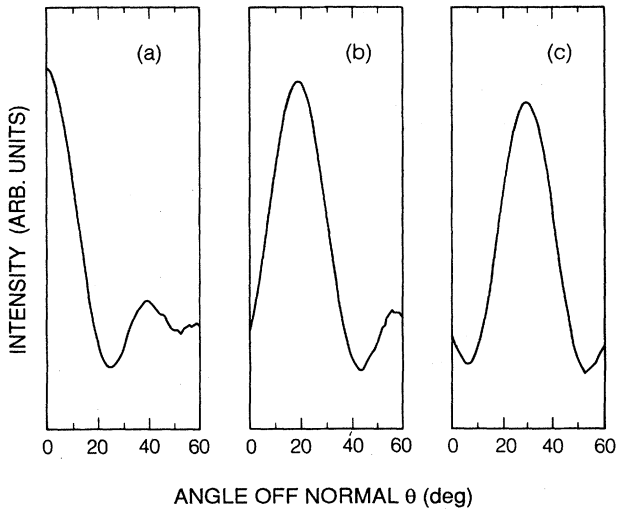

FIG. 4. (a) Calculated polar-angle intensity distribution along the [100] azimuth for hypothetical C electron emission at $E = 950$ eV from a single CO molecule on a top site of Ni(100) with the CO molecule perpendicular to the surface. (b) Same as (a), but the CO molecule is tilted 19° off normal in the [100] azimuth. (c) Same as (b), but tilting 30° off normal.

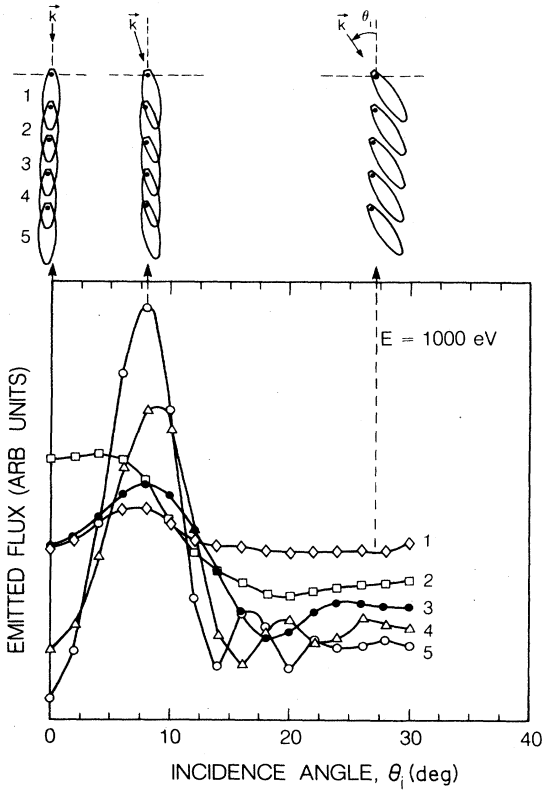

FIG. 5. Emitted-electron flux by different Ni atoms in a chain, due to an incident plane wave at 1000 eV, as function of incident angle. The curves correspond to the atoms numbered 1–5. The upper diagrams show the scattering geometry. The oval attached to each atom represents the atomic-scattering amplitude of Fig. 2.

can be scattered on its way into the crystal; this effect will be explored here.

We have calculated the multiple scattering of a plane wave incident on a surface that has damping. The surface has only one chain of Ni atoms, with a length of five atoms, and it is perpendicular to the surface. As a measure of the distribution of electrons by depth into the surface, Fig. 5 shows the flux of electrons leaving each atom in the chain as a function of incidence direction. This flux is defined as the quantum-mechanical current exiting from each atomic sphere after all multiple scattering has taken place (this involves a two-dimensional solid-angle integration over each atomic sphere with a covalent radius).

In Fig. 5 let us first consider a far off-axis incident direction (far compared to the forward-scattering peak half-width of about 10°; for instance, 27°). Then there is little multiple scattering, because the forward-scattered waves miss the next atoms down the chain. As a result, the flux leaving each atom is mainly determined by the damping and thus decreases exponentially with the depth of the atoms.

At an off-axis angle of 8°, close to the peak half-width, multiple scattering sets in strongly. In this situation, each atom receives not only the undisturbed (although damped) incident plane wave, but also scattered contributions from atoms preceding it in the chain. In a small angular range (about 5°–10° off axis), the result is a surprising amplification: the deeper atoms end up sending out more flux than the shallower atoms, with the fifth atom in Fig. 5 giving out more than any of the preceding ones (ultimately, of course, damping takes over and prevents unlimited amplification). In this situation, forward focusing onto neighbors is active, while defocusing is not yet active. In an Auger experiment, for example, this would imply that most emitted Auger electrons come from deeper in the surface, with a depth distribution as shown in Fig. 5, rather than with an exponential depth distribution given simply by the damping.

Besides amplification, we have also found a focusing enhancement. This occurs when the incident direction is within the peak half-width from the axis direction (i.e., about 5° in Fig. 5). Here focusing of the incident plane wave occurs on the second atom in the chain, while defocusing reduces the contribution reaching the deeper layers, relative to the almost kinetic case shown for far off-axis directions. Figure 6 shows the energy dependence of this focusing enhancement: it is stronger at higher energies. At an actual surface, one may thus preferentially expose atoms in a certain layer by suitable choice of the incident angle.

VII. CONCLUSIONS

We have presented two versions of a multiple-scattering theory developed for electron scattering in chains of atoms. The first version yields self-consistently exact results, while the second is a perturbation expansion that relies on sufficient damping to converge. The first already gives a very efficient computation, in the sense that its computational cost rises only as a small power of the energy and number of phase shifts. The second is even faster, because it only computes the wave field in the immediate neighborhood of the next scatterer, rather than in a large volume around the last scatterer.

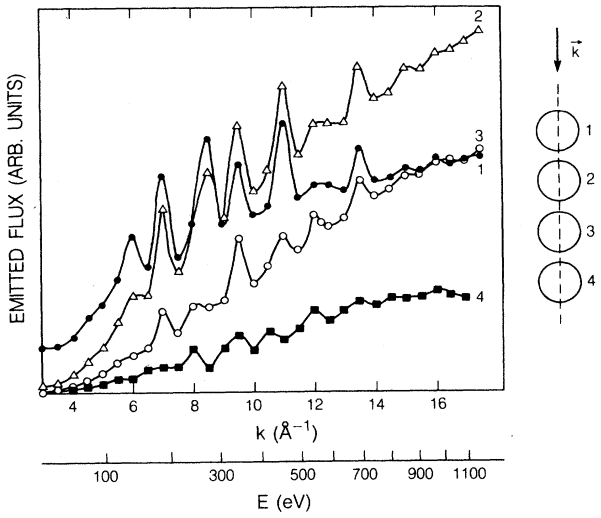

FIG. 6. Emitted-electron flux by different Ni atoms in a chain, due to an incident plane wave, as function of incident energy. The curves correspond to the atoms numbered 1–4. The right-hand diagram shows the on-axis scattering geometry.

We have shown that forward focusing along chains of atoms play a role in a number of important techniques which are sensitive to surface structure. We explore these applications of forward focusing in more detail in separate publications.[23,24]

Focusing on the way into the surface is also possible, as we have shown, and is of significance in Auger-electron spectroscopy. In this case, incident electrons can be preferentially focused with variable effectiveness on atoms at different depths in the surface. Then, Auger electrons are generated with a nonexponential depth distribution.

ACKNOWLEDGMENTS

We are grateful for stimulating discussions with W. F. Egelhoff, Jr., C. S. Fadley, S. A. Chambers, and S. Y. Tong. This work was supported in large part by the U.S. Army Research Office, with institutional support by the Director, Office of Energy Research, Office of Basic Energy Sciences, Materials Sciences Division, of the U.S. Department of Energy under Contract No. DE-AC03-76SF00093. J. J. Barton gratefully acknowledges partial support by IBM.

*Present address: IBM Thomas J. Watson Research Center, P.O. Box 218, Yorktown Heights, NY 10598.

[1]J. B. Pendry, *Low-Energy Electron Diffraction* (Academic, London, 1974).

[2]M. A. Van Hove and S. Y. Tong, *Surface Crystallography by LEED* (Springer-Verlag, Heidelberg, 1979).

[3]M. A. Van Hove, W. H. Weinberg, and C. M. Chan, *Low-Energy Electron Diffraction* (Springer-Verlag, Heidelberg,

1986).
[4]N. Masud, C. G. Kinniburgh, and J. B. Pendry, J. Phys. C **10**, 1 (1977).
[5]P. A. Maksym and J. L. Beeby, Surf. Sci. **110**, 423 (1981).
[6]P. A. Maksym and J. L. Beeby, Surf. Sci. **140**, 77 (1984).
[7]J. J. Barton and D. A. Shirley, Phys. Rev. A **32**, 1019 (1985).
[8]J. J. Barton and D. A. Shirley, Phys. Rev. B **32**, 1892 (1985).
[9]J. J. Barton and D. A. Shirley, Phys. Rev. B **32**, 1906 (1985).
[10]J. J. Barton, S. W. Robey, and D. A. Shirley, Phys. Rev. B **34**, 778 (1986).
[11]P. A. Lee, Phys. Rev. B **13**, 5261 (1976).
[12]J. Stöhr, R. Jaeger, and S. Brennan, Surf. Sci. **117**, 503 (1982).
[13]P. I. Cohen, T. L. Einstein, W. T. Elam, Y. Fukuda, and R. L. Park, Appl. Surf. Sci. **1**, 538 (1978).
[14]R. Rosei and D. Crescenzi, Phys. Rev. B **28**, 1161 (1983).
[15]W. F. Egelhoff, Jr., Phys. Rev. B **30**, 1052 (1984).
[16]W. F. Egelhoff, Jr., Phys. Rev. Lett. **59**, 550 (1987).
[17]S. A. Chambers, S. B. Anderson, and J. H. Weaver, Phys. Rev. B **32**, 581 (1985).
[18]S. A. Chambers, H. W. Chen, I. M. Vitomirov, S. B. Anderson, and J. H. Weaver, Phys. Rev. B **33**, 8810 (1986).
[19]S. A. Chambers, S. B. Anderson, H. W. Chen, and J. H. Weaver, Phys. Rev. B **35**, 2592 (1987).
[20]E. L. Bullock and C. S. Fadley, Phys. Rev. B **31**, 1212 (1985).
[21]J. Osterwalder, E. A. Stewart, D. Cyr, C. S. Fadley, J. M. de Leon, and J. J. Rehr, Phys. Rev. B **35**, 9859 (1987).
[22]M.-L. Xu, J. J. Barton, and M. A. Van Hove, J. Vac. Sci. Technol. A **6**, 2093 (1988).
[23]M.-L. Xu and M. A. Van Hove, Surf. Sci. **207**, 215 (1989).
[24]H. Cronacher, K. Heinz, K. Müller, M.-L. Xu, and M. A. Van Hove, Surf. Sci. (to be published).
[25]S. Y. Tong, H. C. Poon, and D. R. Snider, Phys. Rev. B **32**, 2096 (1985).
[26]J. J. Barton, M.-L. Xu, and M. A. Van Hove, Phys. Rev. B **37**, 10475 (1988).
[27]R. Nozawa, J. Math. Phys. **7**, 1841 (1966).
[28]M. L. Xu, J. J. Barton, and M. A. Van Hove, Lawrence Berkeley Laboratory Report No. 25484, 1988 (unpublished).
[29]J. J. Barton, S. W. Robey, and D. A. Shirley, Phys. Rev. B **34**, 3807 (1986).
[30]V. L. Moruzzi, J. F. Janak, and A. R. Williams, *Calculated Electronic Properties of Metals* (Pergamon, New York, 1978).
[31]S. Y. Tong (private communication).
[32]H. C. Poon and S. Y. Tong, Phys. Rev. B **30**, 6211 (1984).